Green, D. C., Boston, R., Glatzel, S., Lees, M. R., Wimbush, S. C., Potticary, J., Ogasawara, W., & Hall, S. R. (2015). On the Mechanism of Cuprate Crystal Growth: The Role of Mixed Metal Carbonates. *Advanced Functional Materials*, *25*(29), 4700–4707. https://doi.org/10.1002/adfm.201501058

ADVANCED FUNCTIONAL MATERIALS
www.afm-journal.de

Materials Views
www.MaterialsViews.com

On the Mechanism of Cuprate Crystal Growth: The Role of Mixed Metal Carbonates

*David C. Green, Rebecca Boston, Stefan Glatzel, Martin R. Lees, Stuart C. Wimbush, Jason Potticary, Wataru Ogasawara, and Simon R. Hall**

The mechanism of formation of the superconductor $Bi_2Sr_2CaCu_2O_{8+x}$ (Bi-2212) has been an open question since its discovery in 1988. By controlling crystal growth through the use of biopolymers as multivalent cation chelating agents, it is demonstrated through X-ray diffraction and thermogravimetric analysis, that it is the formation of a mixed metal carbonate eutectic that promotes the formation of the target phase. X-ray diffraction experiments, supported by infrared spectroscopy, identify this phase as $(Sr_{1-x}Ca_x)CO_3$. This knowledge allows to further reduce the eutectic melting point by the incorporation of a biopolymer rich in potassium ions, resulting in the scalable formation of Bi-2212 at a temperature 50 °C lower than has been achieved previously.

1. Introduction

The development of high-temperature superconducting (HTS) materials is essential for a future of efficient energy transmission, high-power electrical machines, and novel devices.[1] Several promising families of HTS materials exist, and among these, the rare-earth based *R*-123 family (so-called "second generation" HTS) is presently the leading candidate for widespread application. However, in the face of strong industrial demand for an isotropic, round-wire conductor, recent work[2] on the processing of $Bi_2Sr_2CaCu_2O_{8+x}$ (Bi-2212) has yielded a significant improvement in materials performance that has provided a second contender. Nonetheless, there are still difficulties in the synthesis of phase-pure product in a scalable manner. Successful syntheses of phase-pure superconductors can readily be achieved, although requiring expensive and demanding techniques such as plasma vapor deposition,[3] continuous substrate texturing protocols[4,5] or seed-growth crystal pulling.[6] These techniques are not scalable and therefore preclude them from use in the generation of quantities for commercial exploitation. One possibility to achieve scalability is to produce HTS materials via a sol–gel synthesis.[7–11] Sol–gel synthesis of superconductors generally involves the dispersion of precursor metal salts in solution, often including complexing or stabilizing agents, to form a homogeneous "sol." On calcination, metal salts decompose to single or mixed precursor phases, typically oxides or carbonates, prior to a final reaction yielding the target mixed metal oxide of correct stoichiometry. These syntheses however invariably result in the formation of large crystallites of metal carbonates that are stable throughout calcination that results in the formation of unwanted associate phases and also alters the final stoichiometry of the superconductor.[12] It has been postulated that calcium may be present in the synthesis of Bi-2212 at elevated temperatures as calcium carbonate, which aids in the melting of $SrCO_3$ by forming a low melting point eutectic mixture,[11] which would ensure complete melting and subsequent availability of calcium and strontium ions for Bi-2212 growth, but this has never been conclusively determined.

Here, an in-depth study focusing on the role of the mixed metal carbonate in pure phase Bi-2212 is presented. We demonstrate the significance of mixed metal carbonate through phase evolution studies using X-ray diffraction and thermogravimetric analysis, highlighting the importance of composition

Dr. D. C. Green
School of Chemistry
University of Leeds, Leeds LS2 9JT, UK
Dr. R. Boston
Functional Materials and Devices Group
Materials Science and Engineering
Sir Robert Hadfield Building
University of Sheffield, Sheffield S1 3JD, UK
Dr. S. Glatzel
School of Chemistry
University of Glasgow
Joseph Black Building
University Avenue, Glasgow G12 8QQ, UK
Dr. M. R. Lees
Superconductivity and Magnetism Group
Physics Department
University of Warwick, Coventry CV4 7AL, UK
Dr. S. C. Wimbush
Robinson Research Institute
Victoria University of Wellington
P.O. Box 600, Wellington 6140, New Zealand
J. Potticary, Dr. S. R. Hall
Complex Functional Materials Group
School of Chemistry
University of Bristol, Bristol BS8 1TS, UK
E-mail: simon.hall@bristol.ac.uk
Dr. W. Ogasawara
Department of Bioengineering/Bioenergetics
Nagaoka University of Technology
1603-1 Kamitomiokamachi, Nagaoka, Niigata 940-2137, Japan

DOI: 10.1002/adfm.201501058

Table 1. Summary of wt% biopolymer, heating ramp rate, phase purity, and superconducting critical temperature (T_c) obtained for the Bi-2212 synthesis products of the different biopolymers.

Biopolymer	Biopolymer [wt%]	Ramp [°C min^{-1}]	Phase pure?	T_c [K]
Chitosan	45.4	5	Yes	78
Chitosan	181.5	5	Yes	80
Chitosan	181.5	1	No	80
Dextran	454	5	Yes	78
Dextran	1815	5	Yes	78
Dextran	1815	1	No	79
Xyloglucan	45.4	5	No	78
Xyloglucan	181.5	5	Yes	79
Xyloglucan	181.5	1	No	79
Pectin-K$^+$	45.4	5	No	77
Pectin-K$^+$	181.5	5	Yes	80
Pectin-K$^+$	181.5	1	No	78

and particle size as controlled through the incorporation of biopolymers in to the synthesis of Bi-2212. Enhanced reactivity of the mixed metal carbonate phase was achieved by restricting nucleation and growth to the nanoscale; and enhanced degradation was demonstrated as a function of the changing composition. With this knowledge, acceleration of mixed metal carbonate degradation, and thus eutectic melting point reduction, was achieved through the introduction of a potassium ion-rich biopolymer, resulting in formation of Bi-2212 at a temperature 50 °C lower than has been achieved previously.

2. Biopolymer-Chelated Syntheses of Bi-2212

Full experimental details can be found in the Experimental Section, but briefly, a typical synthesis of $Bi_2Sr_2CaCu_2O_{8+x}$ (Bi-2212) involves the addition of a chelating biopolymer (chitosan, dextran, xyloglucan or pectin-K$^+$) to stoichiometric concentrations of metal nitrates in an ethylenediaminetetraacetic acid (EDTA)-stabilized aqueous solution.[8,13,14] The resultant gel is then dried for 24 h and calcined at 850 °C for 2 h with a 5 or a 1 °C min^{-1} rate of heating. EDTA is added in order to facilitate the full dissolution of $Bi(NO_3)_3$ and prevent the precipitation of associated bismuth phases such as bismuth subnitrate (e.g., $Bi_5O(OH)_9(NO_3)_4$ and other stoichiometries).[15]

Powder X-ray diffraction (pXRD) analysis confirmed the dominant phase to be Bi-2212 (Figure S1, Supporting Information), with a small proportion of $Bi_2Sr_{3-x}Ca_{1+x}O_7$ present as an impurity phase. $Bi_2Sr_{3-x}Ca_{1+x}O_7$ is only present in syntheses using low wt% (45 wt% vs metal nitrates) xyloglucan and pectin-K$^+$ biopolymers, but is not present when higher wt% biopolymer (181.5 wt% vs metal nitrates) is used. No significant quantities of impurities are detected in products from high or low wt% chitosan- and dextran-based precursors. These results are summarized in **Table 1**.

A control sample, generated from a dried metal nitrate solution without any chelating agent under an identical calcination regime is shown (Figure S2, Supporting Information) to have a markedly lower purity of the final product. In this case, Bi-2212 is formed only as a minority phase, with phases such as Bi_2O_3, Sr_2CuO_3, and CuO prevalent, owing to the uncontrolled sintering and growth of these associate phases. This reveals a function of EDTA second to that of chelating agent for solubilising bismuth nitrate, where carbonization at high temperatures either prevents these phases from forming, or provides an effective "cocoon" around associate phases, thereby restricting their growth to the nanoscale and enabling them to melt and be available for further reactions to form the Bi-2212 product. This hypothesis is based on experimental observation reported previously in other biotemplated superconductor syntheses, e.g., refs. [8,16]. When chelating agents such as biopolymers are used, a high purity of the final Bi-2212 product is achieved despite very short dwell times (2 h) and a fast temperature ramp (5 °C min^{-1}) during calcination (Figure S1, Supporting Information). At a slower ramp rate of 1 °C min^{-1} (with the same dwell time and temperature), all biopolymers yield products with greater proportions of impurities (Figure S3, Supporting Information), even at the higher wt% of biopolymer, suggesting slow ramp rates are detrimental to the Bi-2212 synthesis. We attribute this to the breakdown of the carbonaceous cocoon and also to the loss of bismuth from volatile bismuth-rich phases during prolonged heating.

Studies by scanning and transmission electron microscopy (SEM and TEM) reveal the prominent plate-like morphology associated with large blocking layer (i.e., the layer between Cu_2O planes in the unit cell, large classified as >1 nm) perovskite-like superconductors (Figure S4, Supporting Information).[17] Chemical composition and crystallographic structure are confirmed with energy-dispersive X-ray analysis (EDXA) and selected area electron diffraction (SAED), respectively (Figure S5, Supporting Information). In all samples, a high purity of product is observed, with no correlation between particle size and biopolymer content.

Superconductivity in all materials was determined by superconducting quantum interference device (SQUID) magnetometry, with the superconducting critical temperature (T_c) for each product observed from magnetic susceptibility versus temperature measurements (Figure S6, Supporting Information). These revealed that T_c ranged between 77 and 80 K across all the samples. In samples prepared using higher wt% of chitosan, xyloglucan, and pectin-K$^+$, a 1–3 K improvement in T_c is observed. No appreciable difference in T_c is observed for samples prepared from dextran precursors, since the products are phase pure from both higher and lower wt% precursors. Low T_c values obtained from biotemplated Bi-2212 products, and small differences between individual samples, was attributed to the non-optimal and variable degree of oxygenation of $Bi_2Sr_2CaCu_2O_{8+x}$ as a result of static calcination in air (as opposed to flowing oxygen), where optimal T_c (reported between 80 and 95 K) occurs at $x = 0.16$.[18–20]

3. Evolution of the Bi-2212 Phase

In order to ascertain the mechanism of formation of $Bi_2Sr_2CaCu_2O_{8+x}$ (Bi-2212), a phase evolution study was

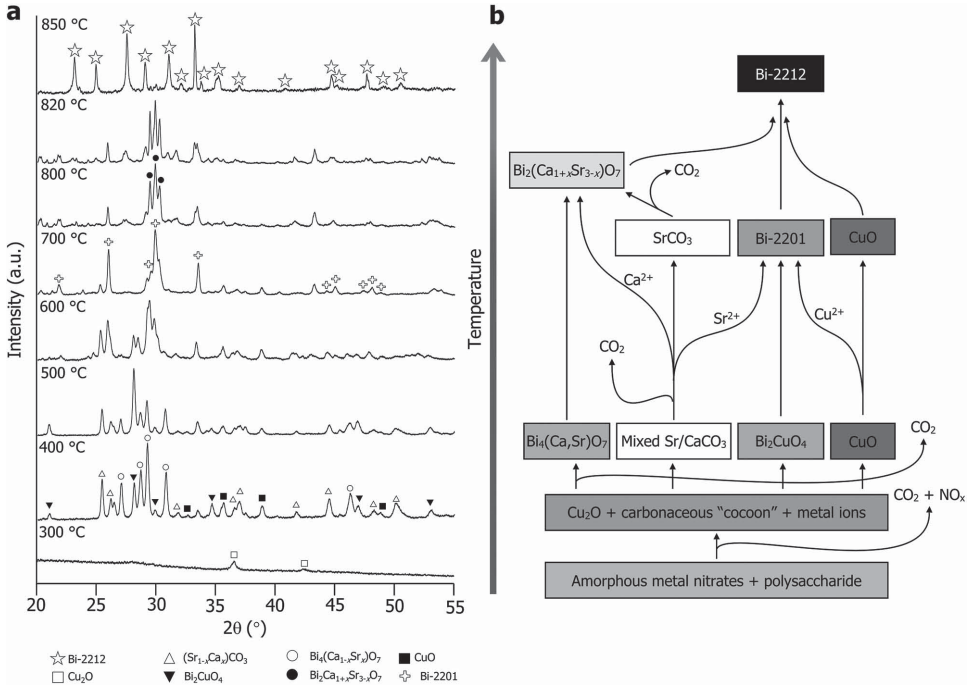

Figure 1. Phase evolution study as a function of temperature. a) pXRD analysis of samples calcined from dextran 1815 wt% precursors at different temperatures revealed the evolution of associate phases leading to final Bi-2212 product. b) Phases observed in each pattern are denoted by the symbols in the legend. This can be summarized graphically as a general mechanism of phase evolution to describe the emergence and fate of associate phases, as well as potential mass transport and outgassing events.

conducted. In a representative study, precursors for Bi-2212 prepared with dextran were calcined with consistent dwell times and heating ramp rates (2 h and 5 °C min^{-1}, respectively) and differing calcination temperatures (300, 400, 500, 600, 700, 800, 820, and 850 °C) (**Figure 1**a) The general phase evolution was determined from identifying the emergence and fate of various associate phases (Figure 1b), and this showed strong agreement with comparative studies with chitosan, xyloglucan, and pectin-K^+ (Figure S7, Supporting Information). Chitosan, dextran, and xyloglucan-rich precursors follow similar phase evolution, with the formation of mixed carbonate $(Sr_{1-x}Ca_x)CO_3$, where x is the molar fraction of Ca^{2+}, denoted x[Ca]; Bi_2CuO_4 or $Bi_{12}CuO_{19}$, CuO and $Bi_4(Sr_{1-x}Ca_x)O_7$ by 400 °C. Xyloglucan and dextran precursors also yield a reduced Cu_2O phase by 300 °C before subsequent oxidation at higher temperature. The mixed carbonate phase remains detectable until 800 °C, while Bi-rich phases and CuO sinter to form a Ca-poor $Bi_2Sr_2CuO_6$ (Bi-2201) phase as well as a Cu-poor $Bi_2Sr_{3-x}Ca_{1+x}O_7$ phase by the same temperature. Between 820 and 850 °C, fully efficient melting of these associate phases takes place to yield the target Bi-2212 phase.

With this unambiguous identification of a mixed metal carbonate phase, we then examined the effect that the potassium ion-rich biopolymer pectin-K^+ had on the synthesis of Bi-2212. The introduction of potassium ions causes depression of the melting point of the mixed carbonate phase, leading to target phase evolution at a lower temperature. Although suggestions of associate phase melting point depression with K^+/Na^+ present during calcination have appeared recently,[16,21–23] the mechanism has not been explicitly demonstrated. Monovalent cation-rich syntheses have also been demonstrated in molten salts,[24,25] thus the nature of the growth described here can be thought of as an amalgam of the two synthetic approaches. Atomic absorption elemental analysis (**Table 2**) confirmed that pectin-K^+ (K^+ = 9.2 wt%) is significantly richer by mass in monovalent cations than any other biopolymer used in this study.

With pectin-K^+ present in the synthesis, only CuO is detected crystallographically at 400 °C. The mixed carbonate phase is detected only by 500 °C as a minor phase before rising to full prominence at 600 °C. Almost complete decomposition has taken place by 700 °C. Bismuth phases (e.g., $Bi_2Sr_{3-x}Ca_{1+x}O_7$, and $Bi_4(Sr_{1-x}Ca_x)O_7$) and Bi-2201 evolve in a similar manner to the other precursors, however almost complete decomposition and sintering of these phases occurs between 700 and 800 °C when Bi-2212 is clearly detected. The addition of pectin-K^+ therefore results in the formation of Bi-2212 at ≈50 °C lower than has been previously reported.

Table 2. Total mass of K^+ and Na^+ in the dry polysaccharide powders determined from atomic absorption analysis. The values were obtained immediately after calibration and post drift corrections.

Polysaccharide	K^+ [mg g^{-1}]	Na^+ [mg g^{-1}]
Chitosan	0.018	0.566
Dextran	0.017	0.013
Xyloglucan	0.729	0.522
Pectin-K^+	92.06	2.245

4. On the Nature of the $(Sr_{1-x}Ca_x)CO_3$ Mixed Metal Carbonate Phase

To track the evolution and degradation of the mixed metal carbonate phase in the complex precursors, a structural study was performed by pXRD on $(Sr_{1-x}Ca_x)CO_3$ products from dextran-rich syntheses of known stoichiometry (**Figure 2**a) in a study similar to previous work to establish the relationship between lattice parameters and composition, or obedience to Vegard's law.[26]

Precursors calcined at 500 °C for 2 h with a 5 °C min^{-1} heating ramp yield the orthorhombic mixed $(Sr_{1-x}Ca_x)CO_3$ phase for $x < 0.5$. This phase resembles calcium-doped strontianite, which has an orthorhombic unit cell (space group *Pmcn*) similar to strontianite ($SrCO_3$) and aragonite ($CaCO_3$). At $x = 0.5$, both orthorhombic and rhombohedral (strontium-doped calcite, space group $R\bar{3}2/c$) are present. Between $x = 0.5$ and $x = 0.75$, the formation of the rhombohedral phase is favored over the orthorhombic. Likewise, between $x = 0.2$ and 0.5, the formation of the orthorhombic phase is favored. This suggests that the cation of highest molar fraction dictates which phase dominates. Since the carbonate phase identified in phase evolution studies is of the orthorhombic phase, it is deduced that $x < 0.5$, and thus it is the orthorhombic phase which is of most interest.

Correlation between changes in lattice parameters and composition is observed from pXRD, where the center of peaks indexed to (111) and (021) in the orthorhombic phase shift to higher 2θ angles (i.e., smaller lattice spacing) with increasing x from $x = 0$ to $x = 0.5$ (Figure 2b, left box). A similar relationship is also observed in the rhombohedral phase, as indicated by a shift of the (104) reflection to lower 2θ with decreasing x (Figure 2b, right box).

In the case of the orthorhombic phase, $d(111)$ is linearly related to x[Ca] in the initial precursor, which suggests full homogeneity of the precursor, and excellent agreement that the orthorhombic $(Sr_{1-x}Ca_x)CO_3$ phase obeys Vegard's law (Figure 2c). The changing chemical composition of the mixed carbonate phase is also characterized by the modified energetics of various vibration modes of the carbonate ion by Fourier transform infrared (FTIR) spectroscopy (Figure S8a,b, Supporting Information). From $x = 0$ to $x = 0.3$, vibration modes ν_3E', ν_1A_1', and ν_4E' increase in energy linearly with x due to a net increase in charge density with higher molar fraction of Ca^{2+} withdrawing electron density from antibonding molecular orbitals in the carbonate ion[27] (Figure S8c, Supporting Information).

Thermal degradation of $(Sr_{1-x}Ca_x)CO_3$ was studied by comparing the composition of crystalline phases after calcination at various dwell temperatures. Under comparable calcination conditions, dextran-rich $(Sr_{1-x}Ca_x)CO_3$ precursors with initial molar ratio tailored to yield $x = 0.1$ were decomposed at 500, 600, and 700 °C (Figure S9, Supporting Information). The orthorhombic phase prevails in all samples. Thermal treatment at higher temperatures results in increasing d-spacings observed from the (111) diffraction peak, but also the emergence of a very minor fraction of CaO produced by separation of Ca^{2+} from $(Sr_{1-x}Ca_x)CO_3$ and formation of the oxide phase as opposed to a separate

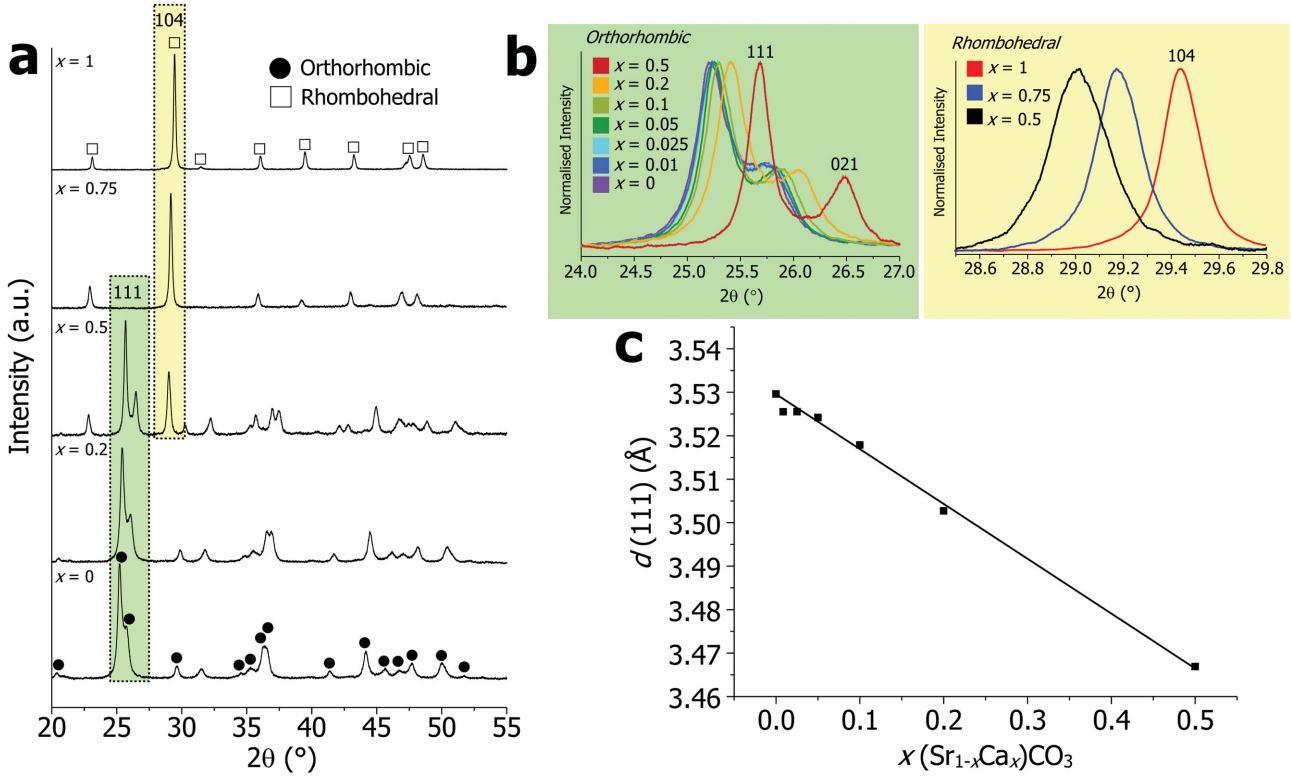

Figure 2. a) $(Sr_{1-x}Ca_x)CO_3$ structural analysis. Dextran-rich precursors for the mixed metal carbonate phase were calcined and the products analyzed by pXRD. b) The relationship between lattice parameters and Ca content x was revealed from the shifting of the (111) and (021) Bragg peaks for the orthorhombic phase (green) and the (104) peak of the rhombohedral phase (yellow); c) $d(111)$ of the orthorhombic phase shifts linearly with x.

carbonate between 600 and 700 °C. This is substantiated by considering the $CaCO_3/CaO/CO_2$ equilibrium at elevated temperatures. While a melting temperature of T_m = 1619 °C is given for calcite, this is unrealistic in an open reaction environment, given the propensity for $CaCO_3$ to decompose to CaO while liberating CO_2. In an open system, effluence of CO_2 away from the reaction shifts the equilibrium towards the oxide product, finally depleting the system of $CaCO_3$. Although a small proportion of CaO is detected at 700 °C, it is concluded that incorporation of Ca^{2+} into the orthorhombic phase inhibits CaO growth. This is highly beneficial in the context of Bi-2212 formation, since the melting temperature of CaO is 2572 °C and would require very long dwell times to process efficiently. It is also the presence of the Ca^{2+} dopant in $SrCO_3$ that depresses stability thereby facilitating melting/mass transport at lower temperatures.

5. The Role of the $(Sr_{1-x}Ca_x)CO_3$ Mixed Metal Carbonate in the Mechanism of Bi-2212 Growth

By using $d(111)$ versus x[Ca] values from pure $(Sr_{1-x}Ca_x)CO_3$ samples as a calibration, the composition of the mixed metal carbonate phase in phase evolution studies of $Bi_2Sr_2CaCu_2O_{8+x}$ (Bi-2212) can be determined (**Figure 3**).

At T = 400 °C, x[Ca] = 0.25, after which x[Ca] decreases linearly with T until 770 °C, where x[Ca] = 0. The same trend can be observed in the FTIR study (Figure S8, Supporting Information), where the ν_3E' vibration mode decreases in energy at higher T as x[Ca] decreases. The same rate of loss of Ca^{2+} is not observed in pure $(Sr_{1-x}Ca_x)CO_3$ samples (Figure S10, Supporting Information), suggesting the Bi-2212 synthesis environment promotes leaching of Ca^{2+}. A small change in x[Ca] is attributed to increasing crystallinity at higher T due to the greater vibrational energy available, and minor leaching resulting in CaO formation as discussed above.

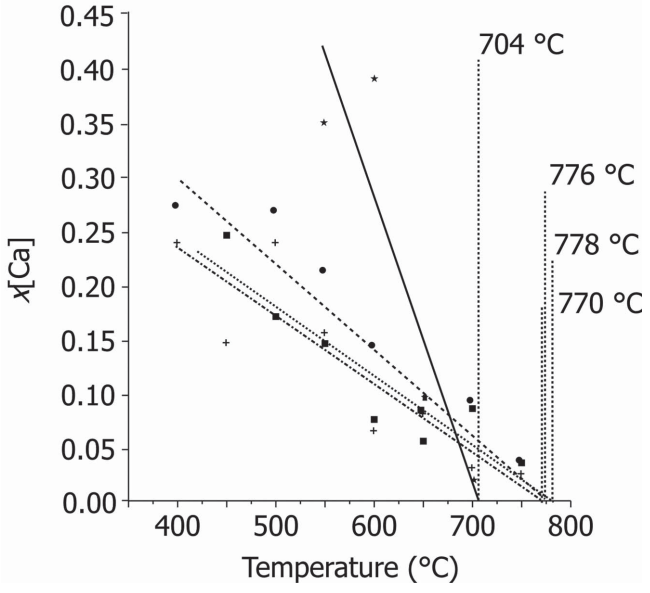

Figure 3. Monitoring changing x in $(Sr_{1-x}Ca_x)CO_3$ with temperature. x[Ca] is determined from pXRD phase evolution study patterns to decrease linearly with T. Chitosan 181.5 wt% (circle data points, dashed line); dextran 1815 wt% (cross data points, dot-dash line) and xyloglucan 181.5 wt% (square data points, dotted line) show similar trends. Pectin-K^+ 181.5 wt% (star data points, solid line) shows a faster decrease in x[Ca] with a lower final degradation temperature.

Similar pXRD analysis of phase evolution studies from chitosan and xyloglucan precursors reveal comparable trends (Figure 3), with $T_{x[Ca]=0}$ = 776 and 778 °C and $x[Ca]_{T=400\,°C}$ = 0.32 and 0.25, respectively, suggesting comparable carbonate decomposition is occurring in similar environments. With K^+-pectin precursors, a faster Ca^{2+} leaching rate is observed (Figure 3). Although crystalline carbonate is detected only between 550 and 700 °C, comparative analysis reveals a much higher Ca^{2+} content ($x[Ca]_{T=550\,°C}$ = 0.4) and a lower $T_{x[Ca]=0}$ of 704 °C. This, coincident with an earlier formation of the target phase, is attributed to the high K^+ content compared to other precursors.

This analysis is in good agreement with data from thermogravimetric analysis and differential scanning calorimetry (TGA/DSC) (Figure S11, Supporting Information). At low T (20–450 °C), from all precursors, mass loss occurs in three stages: between 20 and 100 °C there is a loss of volatiles (i.e., water) (blue), at 200 °C carbonization of organics (polymers, EDTA) occurs together with loss of NO_x following degradation of nitrates (cyan), and at 400–450 °C final combustion of the amorphous carbon matrix takes place (green). At high T (450–1100 °C), after final combustion of the organics, a progressive mass loss occurs with all precursors, with a sudden change in rate at approximately 775 °C, attributed to full degradation of the carbonate phase and initial formation of the Bi-2212 eutectic. DSC reveals extra endothermic activity in pectin-K^+ compared to xyloglucan. A single prominent melting event occurs from xyloglucan beginning at 810 °C (maximum 855 °C), attributed to the Bi-2212 eutectic. An additional earlier lower T endothermic melting event occurs in the presence of pectin-K^+ starting at 720 °C (maximum 780 °C), attributed to a faster K^+-mediated carbonate degradation which depresses the temperature at which Bi-2212 eutectic is formed. This mass loss is attributed to a disproportionately higher rate of loss of Ca^{2+} compared to Sr^{2+} from the $(Sr_{1-x}Ca_x)CO_3$ phase, causing the loss of one CO_2 molecule per metal ion and the subsequent sequestration of Ca^{2+} (and Sr^{2+}) into a developing associate phase. The presence of K^+ increases the rate at which this occurs leading to T_m depression. This phenomenon is summarized in comparison to the general mechanism in **Figure 4**. While the formation and degradation of the mixed carbonate phase is comparable from both K^+-rich and K^+-poor precursors, accelerated degradation of the carbonate resulting in a depressed T_m results in a lower Bi-2212 eutectic.

Finally, to highlight the fate of Ca^{2+} and Sr^{2+} as the carbonate decomposes, a global reaction scheme is shown in **Figure 5**. This details the proportions of different phases versus T, with the proportion taken against the intensity of most intense pXRD peak of each phase. The degradation of the carbonate phase can be observed as the evolution of the strontium rich phase Bi-2201 occurs, between 550 and 600 °C, also accompanied by a reduction in the proportion of the alkali earth metal-poor phase Bi_2CuO_4. It is suggested that the degradation of carbonate leading to formation of oxides occurs with

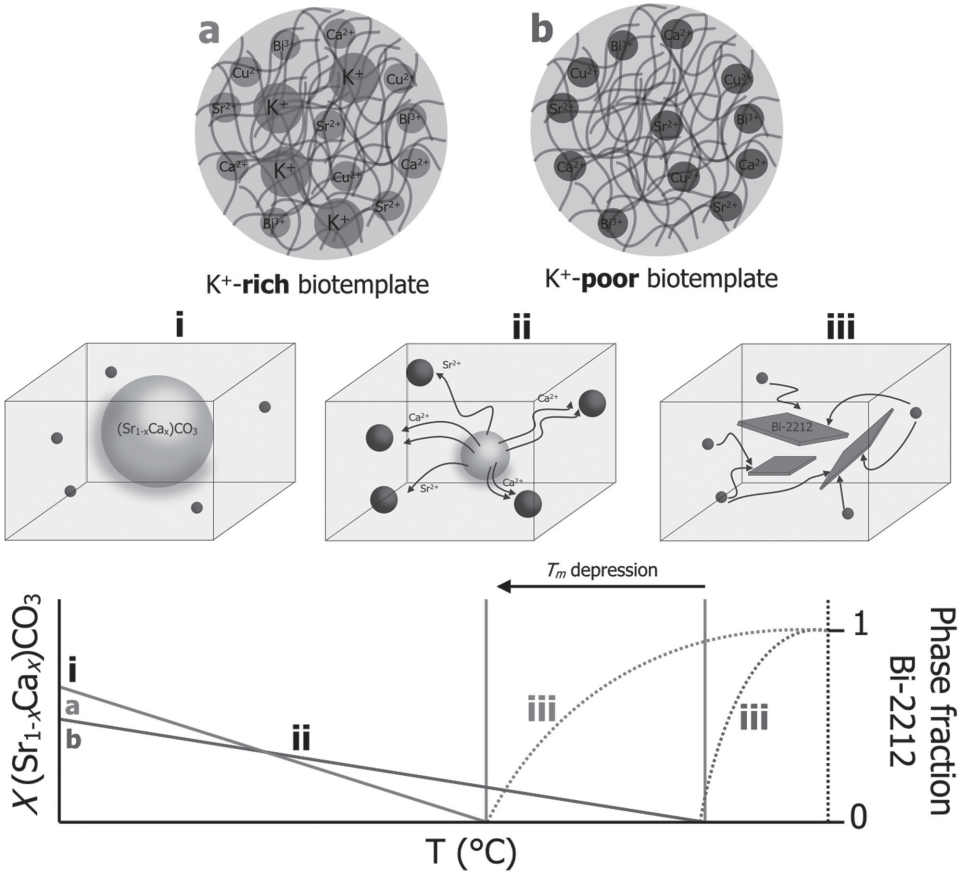

Figure 4. The role of the carbonate phase in Bi-2212 phase evolution. a) Schematic detailing K^+-rich and b) K^+-poor precursors for Bi-2212. The general mechanism involving the carbonate phase is shown in three stages: i) carbonate embedded in associate phase bulk, ii) mass transport of Sr^{2+} and Ca^{2+} to the associate phase upon carbonate degradation, and iii) melting of the associate phase leading to Bi-2212 growth. K^+ reduces the melting temperature T_m of the carbonate phase resulting in Bi-2212 growth at lower T.

the preferential inclusion of strontium into the pre-existing Bi_2CuO_4 phase as opposed to forming a discrete SrO phase. Calcium is not incorporated into a bismuth cuprate phase until approximately 800 °C, where the Bi-2212 phase begins to form. Instead, the fate of calcium after the degradation of carbonate is to sequester into a bismuth oxide $Bi_4Sr_xCa_{1-x}O_7$ to yield a bismuth-alkaline earth oxide with a higher proportion of alkaline earths ($Bi_2Sr_{3-x}Ca_{1+x}O_7$) instead of forming CaO. It must be mentioned that strontium liberated from the carbonate degradation is sequestered into this phase, as well as into Bi_2CuO_4. CuO degradation occurs gradually throughout the heating of the precursor, initially through growth of Bi_2CuO_4, followed by the formation of the Bi-2201 phase as both the carbonate phase and the Ca-containing $Bi_4(Sr_xCa_{1-x})O_7$ transforms to $Bi_2(Sr_{3-x}Ca_{1+x})O_7$ (thus liberating a proportion of Bi^{3+} ions) simultaneously.

6. Conclusion

The mechanism of formation of the superconductor $Bi_2Sr_2CaCu_2O_{8+x}$ (Bi-2212) has been shown for the first time. Through a rigorous study of target phase evolution via pXRD, FTIR, and TGA, we have unambiguously identified the mixed metal carbonate $(Sr_{1-x}Ca_x)CO_3$ as critical to the successful formation of the target phase. Furthermore, we conclude that the introduction of K^+ reduced the melting point of $(Sr_{1-x}Ca_x)CO_3$ by ≈50 °C, enabling the formation of Bi-2212 at lower temperatures than have previously been achieved. Complementary studies also revealed the significance of the chemical

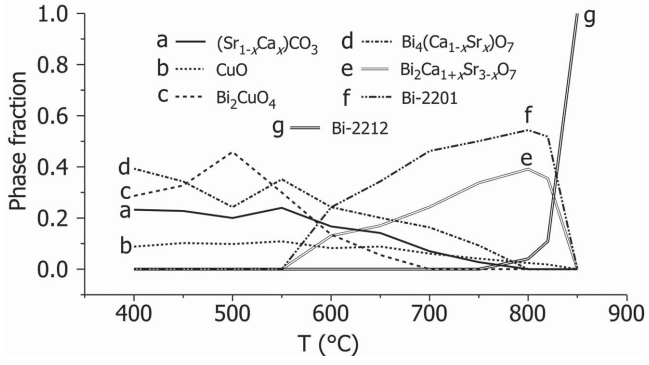

Figure 5. Global reaction diagram showing the mechanism of Bi-2212 growth. Qualitative analysis of pXRD patterns from phase evolution studies of dextran 1815 wt% products reveal the evolution of associate phases before Bi-2212 formation.

composition of $(Sr_{1-x}Ca_x)CO_3$ in preventing the formation of unwanted phases which would inhibit Bi-2212 phase evolution.

It is envisaged that precursor phase control through the use of chelating agents and static molten salt processing can be further extended to other important functional materials in order to improve phase purity, for crystal engineering and as an effective protocol for materials discovery where previously desirable inorganic oxides can be obtained through successful degradation of otherwise stable unwanted phases. Through the enhancement of scalable sol–gel protocols, this also presents economical advantages in industrial applications, where shortened synthesis times, lower heating temperatures and high yields of phase-pure product could reduce manufacturing costs, reduce wastage, and increase metal oxide performance.

7. Experimental Section

Materials and Methods: All the metal nitrates ($Bi(NO_3)_3{\cdot}5H_2O$, $Sr(NO_3)_2$, $Ca(NO_3)_2{\cdot}4H_2O$, and $Cu(NO_3)_2{\cdot}2.5H_2O$), anhydrous ethylenediaminetetraacetic acid (EDTA), chitosan (medium molecular weight, viscosity 200–800 cP when 1 wt% in 1% acetic acid) and esterified pectin from citrus peel (potassium salt) were purchased from Sigma-Aldrich, UK. Dextran (M_r = 75 000) was purchased from Fluka, UK. Glacial acetic acid and ammonium hydroxide solution were purchased from Fisher Scientific, UK. Xyloglucan was a gift from W.O. Deionized water (18.2 MΩ cm^{-1}) was obtained from an in-house Milli-Q PureLab Ultra water purification system. All materials were used as supplied and not purified further.

Production of Aqueous Precursors: 0.4851 g bismuth nitrate pentahydrate (0.1 M), 0.1181 g calcium nitrate tetrahydrate (0.05 M), 0.2116 g strontium nitrate (0.1 M), 0.2326 g copper nitrate pentahemihydrate (0.1 M), and 0.5 g anhydrous EDTA (0.17 M) were suspended in 10 mL deionized water with the addition of 300 µL ammonium hydroxide (1.44 M) before covering and heating to 80 °C while stirring for 5 min to yield a blue solution.

Formation of Polysaccharide Gels: Chitosan, xyloglucan, and pectin-K^+ were solubilized in 50 mL deionized water to yield 2 wt% (i.e., 1 g in 50 mL). For xyloglucan and pectin, dissolution occurs over 2 h at 80 °C under vigorous stirring yielding colorless, homogeneous, viscous solutions. For chitosan, insoluble polysaccharide was suspended in deionized water and vigorously stirred while 600 µL glacial acetic acid was added. Complete dissolution under stirring occurred over 16 h yielding a viscous yellow homogeneous solution. Dextran requires no preliminary treatment. Polysaccharide/Bi-2212 precursor solutions were mixed by stirring at 80 °C for 15 min before gel formation. Typically, 1 mL of Bi-2212 precursor was mixed with 10 mL or 2.5 mL of polysaccharide solution depending on the wt% biopolymer under investigation. For dextran, 1 mL Bi-2212 precursor was added to 2 or 0.5 g dextran and mixed until dissolved to yield a viscous paste. All aqueous precursors were transferred to Petri dishes and dried for 16–24 h. For the $(Sr_{1-x}Ca_x)CO_3$ study precursors, dextran precursors were generated as described above (1 mL Bi-2212 with 0.5 g dextran) from mixtures of 0.4 M $Ca(NO_3)_2$ and 0.4 M $Sr(NO_3)_2$ yielding a mixed nitrate solution of 0.1 M final concentration Ca/Sr^{2+}. The ratio by which they were mixed was dependent on the desired doping of calcium required, i.e., value of x in $(Sr_{1-x}Ca_x)CO_3$.

Calcination Procedures: In a typical calcination for generation of Bi-2212 superconductor, precursors were fired at 850 °C for 2 h in alumina crucibles with a heating ramp of 5 °C min^{-1} yielding a brittle, black solid. Ramp rate and dwell temperature were adjusted as described for the phase evolution study and the slow heating ramp of 1 °C min^{-1}. Precursors and protocols were adjusted for the mixed carbonate studies as described.

Characterization: All powder X-ray diffraction (pXRD) was conducted on ethanoic dispersions of pulverized sample deposited on Si wafers on a Bruker D8 Advance powder X-ray diffractometer equipped with a Cu Kα (λ = 0.154 nm) radiation source and a Lynx-Eye detector. Diffraction patterns were analyzed using the following JCPDS cards for phase identification:

$Bi_{12}CuO_{19}$	00-049-1765
$Bi_{14}Ca_5Sr_7O_{33}$	00-049-0469
$Bi_{14}Ca_9Sr_3O_{33}$	00-049-0471
Bi-2201	00-039-0283
Bi-2212	00-040-0378
$Bi_2Ca_{1+x}Sr_{3-x}O_7$	00-052-1125
Bi_2CuO_4	00–042–0334
$Bi_4(Ca_{1-x}Sr_x)O_7$	00-047-0590
Bismuth subnitrate	00-028-0654
$CaCO_3$ (aragonite)	00-041-1475
$CaCO_3$ (calcite)	00-005-0586
Cu_2O	00-005-0667
CuO	00-045-0937
$SrCO_3$	00-005-0418

Superconducting quantum interference device (SQUID) measurements were conducted in a Quantum Design MPMS-5S or 5T SQUID magnetometer equipped with a 5 T superconducting magnet on pulverized samples placed in gelatine capsules. TEM was conducted on dispersions dried onto carbon coated Cu grids using a JEOL JEM 1200 TEM. Selected area electron diffraction (SAED) patterns were taken with a 4 s exposure onto Kodak TEM film at a camera length of 100 cm. Scanning electron microscopy (SEM) was conducted on desiccated samples mounted on aluminum stubs with carbon pads using a JEOL 5600 SEM operating at various acceleration voltages as appropriate. Energy dispersive X-ray analysis (EDXA) was conducted on TEM or SEM with an ISIS Link analysis module and Oxford Instruments X-ray detection unit. Attenuated total reflection Fourier transform infrared (ATR-FTIR) spectroscopy was conducted on a Perkin Elmer Spectrum One ATR-FTIR spectrometer from dry powders. Thermogravimetric analysis (TGA) combined with DSC was conducted on a Netzsch STA 409 EP simultaneous thermogravimetric analyzer with TASC 414/5 controller system on dry powders placed in alumina crucibles, with heating between room temperature and 1100 °C at a ramp rate of 5 °C min^{-1}.

Supporting Information

Supporting Information including color versions of Figures 1–5 (as Figures S12–S16) is available from the Wiley Online Library or from the author.

Acknowledgements

S.R.H., D.C.G., R.B., and J.P. acknowledge the Engineering and Physical Sciences Research Council (EPSRC), UK (Grant No. EP/G036780/1 for R.B. and J.P.), and the Bristol Centre for Functional Nanomaterials for project funding and the NSQI and Electron Microscopy Group in the School of Chemistry, University of Bristol for the provision of IR and microscopy facilities. S.G. would like to thank Dr. Konrad Siemensmeyer at the Helmholtz-Zentrum Berlin für Materialien und Energie for access to SQUID magnetometry equipment. The magnetometer used by M.R.L. was obtained through the Science City Research Alliance Advanced Materials programme: Creating and Characterizing Next Generation Advanced Materials project, with support from Advantage West Midlands (AWM) and part funded by the European Regional Development Fund

(ERDF). Data accessibility: Raw files from TEM, SEM, XRD and SQUID pertaining to all materials in this work have been placed in the University of Bristol Research Data Repository (www.data.bris.ac.uk/data).

Received: March 17, 2015
Revised: May 19, 2015
Published online: June 25, 2015

[1] S. R. Foltyn, L. Civale, J. L. MacManus-Driscoll, Q. X. Jia, B. Maiorov, H. Wang, M. Maley, *Nat. Mater.* **2007**, *6*, 631.
[2] D. Larbalestier, J. Jiang, U. P. Trociewitz, F. Kametani, C. Scheuerlein, M. Dalban-Canassy, M. Matras, P. Chen, N. C. Craig, P. J. Lee, E. E. Hellstrom, *Nat. Mater.* **2014**, *13*, 375.
[3] X. Zeng, A. V. Pogrebnyakov, A. Kotcharov, J. E. Jones, X. X. Xi, E. M. Lysczek, J. M. Redwing, S. Xu, Q. Li, J. Lettieri, D. G. Schlom, W. Tian, X. Pan, Z.-K. Liu, *Nat. Mater.* **2002**, *1*, 35.
[4] S. Kang, A. Goyal, J. Li, A. A. Gapud, P. M. Martin, L. Heatherly, J. R. Thompson, D. K. Christen, F. A. List, M. Paranthaman, D. F. Lee, *Science* **2006**, *311*, 1911.
[5] J. L. MacManus-Driscoll, A. Kursumovic, J. H. Durrell, S. Harrington, S. C. Wimbush, B. Maiorov, L. Stan, H. Zhou, T. Holesinger, H. Wang, *IEEE Trans. Appl. Supercond.* **2009**, *19*, 3180.
[6] X. Yao, M. Egami, Y. Namikawa, T. Mizukoshi, Y. Shiohara, S. Tanaka, *J. Cryst. Growth.* **1996**, *165*, 198.
[7] A. Kareiva, M. Karppinen, L. Niinistä, *J. Mater. Chem.* **1994**, *4*, 1267.
[8] S. R. Hall, *Adv. Mater.* **2006**, *18*, 487.
[9] Y. Zhang, H. Yang, M. Li, B. Sun, Y. Qi, *CrystEngComm* **2010**, *12*, 3046.
[10] D. C. Green, S. Glatzel, A. M. Collins, A. J. Patil, S. R. Hall, *Adv. Mater.* **2012**, *24*, 5767.
[11] G. R. Paz-Pujalt, *Phys. C* **1990**, *166*, 177.
[12] T. Araki, I. Hirabayashi, *Supercond. Sci. Technol.* **2003**, *16*, R71.
[13] A. Tampieri, G. Celottia, S. Lescaa, G. Bezzib, T. M. G. La Torrettab, G. Magnanib, *J. Eur. Ceram. Soc.* **2000**, *20*, 119.
[14] J. Fransaer, J. R. Roos, L. Delaey, O. Van Der Biest, O. Arkens, J. P. Celis, *J. Appl. Phys.* **1989**, *65*, 3277.
[15] L. Miersch, M. Schlesinger, R. W. Troff, C. A. Schalley, T. Rüffer, H. Lang, D. Zahn, M. Mehring, *Chem. Eur. J.* **2011**, *17*, 6985.
[16] Z. A. C. Schnepp, S. C. Wimbush, S. Mann, S. R. Hall, *Adv. Mater.* **2008**, *20*, 1782.
[17] J. L. Macmanus-Driscoll, S. C. Wimbush, *IEEE Trans. Appl. Supercond.* **2011**, *21*, 2495.
[18] H. Takagi, H. Eisaki, S. Uchida, A. Maeda, S. Tajima, K. Uchinokura, S. Tanaka, *Nature* **1988**, *332*, 236.
[19] P. Krishnaraj, M. Lelovic, N. G. Eror, U. Balachandran, *Physica C* **1995**, *246*, 271.
[20] N. Miyakawa, P. Guptasarma, J. Zasadzinski, D. Hinks, K. Gray, *Phys. Rev. Lett.* **1998**, *80*, 157.
[21] Z. Zhang, S. C. Wimbush, A. Kursumovic, H. Wang, J. H. Lee, H. Suo, J. L. MacManus-Driscoll, *CrystEngComm* **2012**, *14*, 5765.
[22] Z. Zhang, S. C. Wimbush, A. Kursumovic, H. Suo, J. L. MacManus-Driscoll, *Cryst. Growth Des.* **2012**, *12*, 5635.
[23] G. Balestrino, E. Milani, A. Paoletti, A. Tebano, Y. H. Wang, A. Ruosi, R. Vaglio, M. Valentino, P. Paroli, *Appl. Phys. Lett.* **1994**, *64*, 1735.
[24] Y. Saito, H. Takao, T. Tani, T. Nonoyama, K. Takatori, T. Homma, T. Nagaya, M. Nakamura, *Nature* **2004**, *432*, 84.
[25] C. Xu, L. Zhen, R. Yang, Z. L. Wang, *J. Am. Chem. Soc.* **2007**, *129*, 15444.
[26] W. H. Casey, L. A. Chai, A. Navrotsky, P. A. Rock, *Geochim. Cosmochim. Acta* **1996**, *60*, 933.
[27] J. M. Alía, Y. Díaz de Mera, H. G. M. Edwards, P. González Martín, S. López Andres, *Spectrochim. Acta Part A: Mol. Biomol. Spectrosc.* **1997**, *53*, 2347.